INTERNATIONAL JOURNAL FOR NUMERICAL METHODS IN FLUIDS
Int. J. Numer. Meth. Fluids 2004; **46**:921–937
Published online 27 September 2004 in Wiley InterScience (www.interscience.wiley.com). DOI: 10.1002/fld.787

Simulation of lid-driven cavity flows by parallel lattice Boltzmann method using multi-relaxation-time scheme

J.-S. Wu*,†,‡ and Y.-L. Shao§

Department of Mechanical Engineering, National Chiao-Tung University, Hsinchu 30050, Taiwan

SUMMARY

Two-dimensional near-incompressible steady lid-driven cavity flows ($Re = 100$–$7{,}500$) are simulated using multi-relaxation-time (MRT) model in the parallel lattice Boltzmann BGK Bhatnager–Gross–Krook method (LBGK). Results are compared with those using single-relaxation-time (SRT) model in the LBGK method and previous simulation data using Navier–Stokes equations for the same flow conditions. Effects of variation of relaxation parameters in the MRT model, effects of number of the lattice points, improved computational convergence and reduced spatial oscillations of solution near geometrically singular points in the flow field using LBGK method due to MRT model are highlighted in the study. In summary, lattice Boltzmann method using MRT model introduces much less spatial oscillations near geometrical singular points, which is important for the successful simulation of higher Reynolds number flows. Copyright © 2004 John Wiley & Sons, Ltd.

KEY WORDS: lattice Boltzmann BGK method; multi-relaxation-time; single-relaxation-time

1. INTRODUCTION

The lattice Boltzmann equation (LBE) using relaxation technique was introduced by Higuerea and Jimenez [1] to overcome some drawbacks of lattice gas automata (LGA) such as large statistical noise, limited range of physical parameters, non-Galilean invariance, and implementation difficulty in three-dimension problem. In the original derivation of LBE using relaxation concept, it was strongly connected to the underlying LGA. But it was soon recognized that it could be constructed independently [2]. Since then, the lattice Boltzmann methods (LBM) have received considerable attention as an alternative to traditional computational fluid dynamics for simulating certain complex flow problems; see References [3–5] and references cited therein. The simplest LBE is the lattice Bhatnager–Gross–Krook (LBGK) equation [6], based on a single-relaxation-time (SRT) approximation. Due to the extreme simplicity, the

*Correspondence to: J.-S. Wu, Department of Mechanical Engineering, National Chiao-Tung University, 1001 Ta-Hsueh Road, Hsinchu 30050, Taiwan.
†E-mail: chongsin@cc.nctu.edu.tw
‡Associate professor.
§Graduate research assistant.

Received 11 July 2003
Revised 19 June 2004

lattice BGK (LBGK) equation [7] has become the most popular lattice Boltzmann model in spite of its deficiencies, for example, in simulating high-Reynolds numbers flow.

In the LBM, fluid is modelled by particles moving on a regular lattice. At each time step particles propagate to neighbouring lattice sites and re-distribute their velocities in a local collision phase. The inherent locality of the scheme makes it perfect for parallel computing [8], whose advantage will be taken in the current study. Through Chapman–Enskog multi-scale expansion [9], the complicated, non-linear compressible Navier–Stokes equations can be recovered from the simple, linear LBGK equation based on the assumptions that, first, Mach number is small, and, second, the density varies slowly in the flow field. Thus, the LBM has been applied mostly to compute the flow field in near-incompressible limit. In particular, the LBGK method has been successfully applied to problems of near-incompressible flows through porous media e.g. References [10–12], multiphase flows e.g. References [13–15] and dynamics of droplet breakup e.g. References [16, 17], to name a few.

However, there exist some deficiencies in solving higher Reynolds number incompressible flow problems or resolving flow fields near geometrically singular points using SRT LBM [18, 19]. On one hand, the fluid density is required to be nearly constant for nearly incompressible flows and the pressure is proportional to the local density field. On the other hand, pressure and shear stress are singular near the geometrically singular points (e.g. sharp corners). Hence, it often causes unphysical, strong local spatial oscillations near these singular points, which turns out to contaminate the flow field far away from these singular points. Previous work originally developed by D'Humieres [19], and further extended by Lallemand and Luo [20] suggests that the use of a MRT model can improve the numerical stability and reduce dramatically the unphysical oscillations for some simple flows. They concluded that using MRT model in the LBM in these simple flows can significantly reduce the spatial oscillation near the singular points and improves the quality of the solution at higher Reynolds number. However, there is no systematic study in revealing the limits of applying the MRT model in the LBM for higher Reynolds number flows, which have complicated flow features.

A lid-driven cavity flow is selected as the test problem because it has geometrically singular points in the flow, but geometrically simple enough considering implementation of boundary conditions, which otherwise complicates the evaluation of MRT scheme in LBM. In addition, this flow is very complicated in flow structure as Reynolds number increases to some extent. In summary, the objectives of the current research are to implement and to evaluate the parallel LBM by using MRT technique by comparing the results of an upper, lid-driven cavity flow with those by LBM using SRT technique and previous results using Navier–Stokes equations.

2. NUMERICAL METHOD

2.1. Lattice Boltzmann method with SRT model

LBM method solves the microscopic kinetic equation for particle distribution $f(x, v, t)$, where x and v is the particle position and velocity vector, respectively, in phase space (x, v) and time t, where the macroscopic quantities (velocity and density) are obtained through moment integration of $f(x, v, t)$. The most popular used LBM equation is the SRT LBGK model [7], and listed as follows:

$$f_i(\bar{x} + \bar{e}\Delta t, t + \Delta t) - f_i(\bar{x}, t) = -\omega[f_i(\bar{x}, t) - f_i^{\mathrm{eq}}(\bar{x}, t)] \tag{1}$$

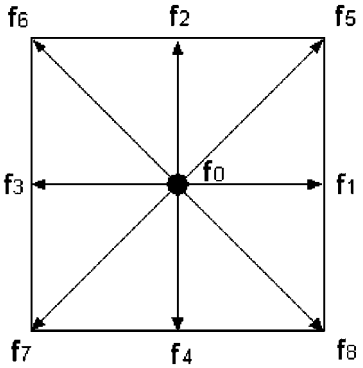

Figure 1. The 9-velocity LBE model on the 2-D square lattice.

where $f_i(\bar{x},t)$ and $f_i^{\mathrm{eq}}(\bar{x},t)$ are the particle distribution function and the equilibrium particle distribution function of the ith discrete particle velocity v_i, respectively, $\bar{e}$ is a discrete velocity vector. Note that $\omega=\Delta t/\tau$ is the collision frequency (Δt is the advancing time step and τ is the collision relaxation time).

The 9-velocity LBE model on the 2-D square lattice (Figure 1), denoted as the D2Q9 model, is used in the current study for simulating the steady lid-driven cavity flow. Let $c=\Delta x/\Delta t=\Delta y/\Delta t$ be the lattice streaming speed (Δx and Δy is the distance a particle moves of grid spacing) for isothermal near-incompressible flows, the equilibrium distribution function can be derived as the following form [9]:

$$f_i^{\mathrm{eq}}(\bar{x},t)=\rho w_i\left[1+\frac{3}{c^2}\,\bar{e}_i\cdot\bar{u}+\frac{9}{2c^4}\,(\bar{e}_i\cdot\bar{u})^2-\frac{3}{2c^2}\,\bar{u}\cdot\bar{u}\right] \tag{2}$$

where w_i is a weighting factor and $\bar{u}$ is the fluid velocity. In addition, the discrete velocities for D2Q9 model are

$$\bar{e}_i=\begin{cases}(0,0), & i=0,\text{rest particle}\\ (\pm c,0),(0,\pm c), & i=1,2,3,4\\ (\pm c,\pm c), & i=5,6,7,8\end{cases} \tag{3}$$

and the values of the weighting factors w_i are

$$w_i=\begin{cases}4/9, & i=0,\text{rest particle}\\ 1/9, & i=1,2,3,4\\ 1/36, & i=5,6,7,8\end{cases} \tag{4}$$

The density and velocities can be computed simply by moment integration as

$$\rho = \sum_i f_i \tag{5}$$

$$\bar{u} = \frac{1}{\rho} \sum_i \bar{e}_i f_i \tag{6}$$

Application of the multi-scale technique (Chapman–Enskog expansion) yields the Navier–Stokes equation with the pressure $p = \rho c_s^2$, where $c_s = c/\sqrt{3}$, and an advection term with Galilean invariance. The viscosity of the simulated fluid is $v = \Delta t(1/\omega - 1/2)c_s^2 = (\tau - 1/2\Delta t)c_s^2$. However, the simplicity has to pay the price of necessarily using square lattices of constant spacing ($\Delta x = \Delta y$) and consequently lead to the unity of the Courant–Fridrich–Levy (CFL) number due to $\Delta x = \Delta y = \Delta t$. From here on we shall use the units of $\Delta x = 1$, $\Delta y = 1$ and $c = 1$ such that all the relevant quantities are dimensionless.

With the choice of viscosity in the above, Equation (1) is formally a second order method (excluding the boundary conditions) for solving near-incompressible flows [9]. Physical and numerical constraints require that $\omega < 2$. In the current study, $\omega = 1.9$ unless otherwise specified. In general, Equation (1) is solved in two steps:

collision step:

$$f_i^*(\bar{x}, t + \Delta t) = f_i(\bar{x}, t) - \omega[f_i(\bar{x}, t) - f_i^{\text{eq}}(\bar{x}, t)] \tag{7a}$$

streaming step:

$$f_i(\bar{x} + \bar{e}_i, t + \Delta t) = f_i^*(\bar{x}, t + \Delta t) \tag{7b}$$

which is known as the LBGK method [5]. Note that, in the above, $*$ denotes the post-collision values. It is obvious that the collision process is completely localized, and the streaming step requires little computational effort by advancing the data from neighboring lattice points that makes Equation (1) perfect for parallel implementation, which will be shown in detail later.

Previous experience in obtaining solutions at higher Reynolds numbers using SRT model of the LBE method has shown that the solution field (u, v, p) often exhibits spurious spatial oscillations in regions of large gradient such as stagnation point and sharp concave corners [18]. For example, it has shown that the serious spatial oscillations of pressure field can be clearly observed at Reynolds number of 5000 with 256×256 lattice points at the upper two concave corners [18]. Depending upon the geometry and flow problem, such spatial oscillation may even propagate to contaminate the flow solutions in the regions far away from the singular points. In addition, the spatial oscillations in the solution can strongly affect the computational stability and convergence rate. Of course, the LBE using SRT model can always improve its computational stability and convergence by increasing the number of lattice points in the computational domain, although it is not recommended in general. Therefore, to develop a similar LBE technique but simple enough in implementation is strongly required to resolve the above-mentioned deficiencies.

2.2. Lattice Boltzmann method with MRT model

Recently, Lallemand and Luo [20] suggested that the use of a MRT model could improve the numerical stability and reduce dramatically the unphysical oscillations for some simple flows.

They have performed detailed theoretical analysis on the dispersion, dissipation and stability characteristics of a generalized lattice Boltzmann equation model proposed by d'Humieres [19]. They have found that the MRT model is equivalent to the SRT model in the long wavelength (low wave number) limit for macroscopic variables of interest in various simple flows through the linearized analysis [20]. Difference between two relaxation models is identified as a high-order effect (short wavelength limit), which can hardly detected in simple flows. It is well known that geometrically and mathematically singular points can adversely affect the flow solution in short wavelength limit. We would thus expect, at least, the solution of MRT model near the singular point is appreciably different from that of SRT model. For convection-dominated flows, the local difference near the singularities may also lead to large differences in flow regimes far away. Thus, it is important to understand how the solution using MRT model is different from that using SRT model. In addition, it is potentially useful to compute flows at higher Reynolds numbers using MRT model in LBM. In what follows, we will briefly summarize the important features of MRT model [20] as compared with those of SRT model.

Lallemand and Luo [20] have defined a new column vector of macroscopic variables $\bar{R}=(\rho, e, \varepsilon, j_x, q_x, j_y, q_y, p_{xx}, p_{xy})^{\mathrm{T}}$ and $\bar{R}$ can be related to the column vector of $\bar{F}=(f_0, f_1, f_2, f_3, f_4, f_5, f_6, f_7, f_8)^{\mathrm{T}}$ as follows:

$$\bar{R}=\begin{bmatrix}\rho\\ e\\ \varepsilon\\ j_x\\ q_x\\ j_y\\ q_y\\ p_{xx}\\ p_{xy}\end{bmatrix}=\begin{bmatrix}1 & 1 & 1 & 1 & 1 & 1 & 1 & 1 & 1\\ -4 & -1 & 2 & -1 & 2 & -1 & 2 & -1 & 2\\ 4 & -2 & 1 & -2 & 1 & -2 & 1 & -2 & 1\\ 0 & 1 & 1 & 0 & -1 & -1 & -1 & 0 & 1\\ 0 & -2 & 1 & 0 & -1 & 2 & -1 & 0 & 1\\ 0 & 0 & 1 & 1 & 1 & 0 & -1 & -1 & -1\\ 0 & 0 & 1 & -2 & 1 & 0 & -1 & 2 & -1\\ 0 & 1 & 0 & -1 & 0 & 1 & 0 & -1 & 0\\ 0 & 0 & 1 & 0 & -1 & 0 & 1 & 0 & -1\end{bmatrix}\begin{bmatrix}f_0\\ f_1\\ f_2\\ f_3\\ f_4\\ f_5\\ f_6\\ f_7\\ f_8\end{bmatrix}=\bar{\bar{M}}\bar{F} \tag{8}$$

where $\bar{\bar{M}}$ is a 9×9 matrix transforming $\bar{F}$ to $\bar{R}$. In the column vector $\bar{R}$, ρ is the fluid density, ε is related to the square of the energy e, j_x and j_y are the mass flux in two directions, q_x and q_y correspond to the energy flux in two directions, and p_{xx} and p_{xy} correspond to the diagonal and off-diagonal component of the viscous stress tensor. One immediate advantage of the MRT model is that macroscopic variables of interest can be obtained readily by simply performing the matrix multiplication $\bar{\bar{M}}\bar{F}$ if $\bar{F}$ is known. In addition, due to the conservation of mass and momentum before and after particle collision, the total mass and momentum should not relax at all. However, Equation (7a) in standard LBGK method requires all f_i's are relaxed at the same rate and, hence, all macroscopic quantities of interest. Physically speaking, different physical modes should have different relaxation rates. By taking this into account in the MRT model, based on Equation (7a), the collision procedure for $\bar{R}^*$ is performed

as follows:

$$\bar{R}^* = \left\{ \begin{array}{c} \rho^* = \rho - s_1(\rho - \rho^{\mathrm{eq}}) \\ e^* = e - s_2(e - e^{\mathrm{eq}}) \\ \varepsilon^* = \varepsilon - s_3(\varepsilon - \varepsilon^{\mathrm{eq}}) \\ j_x^* = j_x - s_4(j_x - j_x^{\mathrm{eq}}) \\ q_x^* = q_x - s_5(q_x - q_x^{\mathrm{eq}}) \\ j_y^* = j_y - s_6(j_y - j_y^{\mathrm{eq}}) \\ q_y^* = q_y - s_7(q_y - q_y^{\mathrm{eq}}) \\ p_{xx}^* = p_{xx} - s_8(p_{xx} - p_{xx}^{\mathrm{eq}}) \\ p_{xy}^* = p_{xy} - s_9(p_{xy} - p_{xy}^{\mathrm{eq}} \end{array} \right\} = \bar{R} - \bar{\bar{S}}(\bar{R} - \bar{R}^{\mathrm{eq}}) \tag{9}$$

where $*$ denotes the post-collision state, $\bar{\bar{S}}$ is the 9×9 diagonal matrix, which will be shown later. In $\bar{\bar{S}}$, $s_1 = s_4 = s_6 = 0$ enforces mass and momentum conservation before and after collision. Note that the equilibrium values in $\bar{R}^*$ can be written as [20]

$$\begin{aligned} e^{\mathrm{eq}} &= -2\rho + 3(u^2 + v^2) \\ \varepsilon^{\mathrm{eq}} &= \rho - 3(u^2 + v^2) \\ q_x^{\mathrm{eq}} &= -u \\ q_y^{\mathrm{eq}} &= -v \\ p_{xx}^{\mathrm{eq}} &= u^2 - v^2 \\ p_{xy}^{\mathrm{eq}} &= uv \end{aligned} \tag{10}$$

Before the streaming step, Equation (7b), is performed, one needs to transform the post-collision values, $\bar{R}^*$, back to $\bar{F}^*$ by using Equation (9) as

$$\bar{F}^* = \bar{\bar{M}}^{-1}\bar{R}^* = \bar{F} - \bar{\bar{M}}^{-1}\bar{\bar{S}}(\bar{R} - \bar{R}^{\mathrm{eq}}) \tag{11}$$

where $\bar{\bar{S}}$ is the diagonal matrix,

$$\bar{\bar{S}} = \begin{bmatrix} 0 & 0 & 0 & 0 & 0 & 0 & 0 & 0 & 0 \\ 0 & s_2 & 0 & 0 & 0 & 0 & 0 & 0 & 0 \\ 0 & 0 & s_3 & 0 & 0 & 0 & 0 & 0 & 0 \\ 0 & 0 & 0 & 0 & 0 & 0 & 0 & 0 & 0 \\ 0 & 0 & 0 & 0 & s_5 & 0 & 0 & 0 & 0 \\ 0 & 0 & 0 & 0 & 0 & 0 & 0 & 0 & 0 \\ 0 & 0 & 0 & 0 & 0 & 0 & s_7 & 0 & 0 \\ 0 & 0 & 0 & 0 & 0 & 0 & 0 & s_8 & 0 \\ 0 & 0 & 0 & 0 & 0 & 0 & 0 & 0 & s_9 \end{bmatrix} \tag{12}$$

Finally, the streaming step for all f_i's in the MRT model is performed exactly the same as in the standard LBGK model using Equation (7b).

Lallemand and Luo [20] have shown that the MRT model can reproduce the same viscosity as that by SRT model if we set $s_8 = s_9 = 1/\tau$. Once this is decided, the rest of the relaxation parameters (s_2, s_3, s_5 and s_7) for different physical modes can then be chosen more flexibly. In Reference [20], they recommended the values to be slightly greater than unity. In this research, we will make some sensitivity study of these parameters in the current test case to see if complicated flow has different optimum values. Finally, it is worthy to note that the MRT model reduces to the SRT model by simply setting $s_2 = s_3 = s_5 = s_7 = s_8 = s_9 = 1/\tau$.

2.3. Parallel implementation of lattice Boltzmann method

Due to the locality of collision (or relaxation) in the LBM, it is highly suitable for parallel computing. Neighbouring lattice points are involved in the LBM only during the streaming (or moving) process, as shown in Equation (7b). Minimum communication as compared with computation is expected; thus, it is natural to apply physical domain decomposition for parallel implementation of LBM. Computational domain is decomposed evenly using the fact that computational time of LBM is approximately proportional to the lattice points in each processor. All results shown later are computed on an 8-node PC-Cluster system, running at 1 GHz for each processor, unless otherwise specified. Parallel efficiency can be nearly 100% in the current test case using 8 processors. Detailed analysis of parallel performance of different parallel implementations will be reported elsewhere.

2.4. Boundary conditions

2.4.1. Stationary wall boundary conditions. How to properly implement the wall boundary conditions within LBM framework is still an ongoing research topic e.g. Reference [21] and reference cited therein. The most often-used scheme is the so-called 'bounce back' scheme, which has been argued that it is only of first-order accuracy as compared with of second-order accuracy for LBM formulation. However, it was recently shown that the error is sufficiently small if the relaxation parameter ω (or $1/\tau$) is chosen to be close enough to 2 [21]. Thus, we believe that the bounce-back boundary conditions in the current study shall not influence the order of accuracy of LBM using SRT and MRT models if we choose ω to be within some range.

2.4.2. Moving wall boundary conditions. For the current problem, we have assumed equilibrium distribution function at the upper moving plate, which is computed by substituting the uniform plate velocity into Equation (2) and the initial density assignment. After streaming, the velocity at the top plate is reinforced to be the uniform plate velocity and then the equilibrium distribution function is reevaluated using the fixed plate velocity and the updated density at the plate. In the current study, the upper two corner lattice points are considered as the part of the moving plate. The uniform top plate velocity is $U = 0.1$, considering the validity of using LBM in simulating near-incompressible flows.

3. RESULTS AND DISCUSSIONS

To clearly demonstrate and test the advantages of LBM using MRT model over that using SRT model, we compute a steady, upper lid-driven flow ($Re = 100$–7500) by LBM using both

MRT and SRT models. We compare various macroscopic variables of interest in regions of both large and small gradients. In addition, results from the LBM using MRT and SRT models are compared with those of N–S solvers by Ghia *et al.* [22] where it is appropriate. For all the cases presented in this paper, steady-state solution is assumed only when the absolute value of relative difference of the velocities (both u and v) at all lattice points is less than 10^{-5} for successive 10 000 time steps.

Figure 2 demonstrates the typical test of grid sensitivity (64×64 and 256×256 lattice points) by comparing the velocity profiles ($Re = 1000$) at the centreline of the cavity for both SRT and MRT models with the data by Ghia *et al.* [22], which has been considered to be the most comprehensive computation for the impressible lid-driven cavity flow. It is clearly shown that the difference of velocity distributions between the current study and Ghia *et al.* [22] is very small at 256×256 lattice points. Also the difference between MRT and SRT models is nearly undistinguished at this Reynolds number of 1000. Similar trends are found for other Reynolds numbers up to 7500 for both MRT and SRT models. Thus, all results discussed in the followings are computed using 256×256 lattice points, unless otherwise specified.

Figure 3 shows the simulated streamline for Reynolds numbers of 100, 1000 and 7500 for both SRT and MRT models. Since the upper plate moves into the right-hand direction, the major vortex in the center circulates in clockwise direction as expected. In addition to the major vortex, there appear two minor vortices circulating counterclockwise in the lower cavity corners ($Re = 1000$ and 7500), the third minor vortex circulating counterclockwise in the upper left-hand corner ($Re = 7500$), and the fourth minor vortex circulating clockwise in the lower right-hand corner at $Re = 7500$. Note that only MRT model is able to predict the fourth minor vortex in the lower right-hand corner, which is also a geometrically singular point, while SRT model fails to predict the fourth minor vortex at this corner. In addition, the sizes of the minor vortices increase with increasing Reynolds numbers. Generally speaking, the overall flow structures (streamlines) predicted by the SRT and MRT models are very similar to those predicted by Ghia *et al.* [22], except some differences near the corners, which can be amplified later by looking at other flow properties.

Simulated location (x- and y-co-ordinate) of major central vortex as a function of Reynolds numbers by both SRT and MRT models along with previous data by Ghia *et al.* [22] using is illustrated in Figure 4. For low Reynolds number (e.g. $Re = 100$), the centre of the primary vortex is located near the right-hand corner of the cavity. As Reynolds number increases, the primary vortex centre moves towards the geometric centre of the cavity. Maximum stream function values of the present study for the primary vortex at different Reynolds numbers are listed in Table I along with the previous data by Ghia *et al.* [22]. The results of the present work and that of Ghia *et al.* [22] are in excellent agreement within 0.8% for all Reynolds numbers, except for $Re = 2000$, where the data is provided by Ghia *et al.* [22]. In addition, excellent agreement between STR and MRT models is also found.

Figure 5 shows the vorticity distribution using both SRT and MRT models at different Reynolds numbers ($Re = 100$, 1000 and 7500). It is clear that the vorticity distribution using these two models is approximately the same for $Re = 100$ and 1000. However, for $Re = 7500$ (similarly for $Re = 5000$), there exists obvious vorticity 'jiggles' around the upper two cavity corners using SRT model, especially the left-hand one due to the geometrical singularity at this corner. Most importantly and interestingly, this vorticity 'jiggles' is not only localized at the corner, but also it has contaminated the solution far away from the corner, as shown clearly in Figure 5(f). The situation is even worse at $Re = 10\,000$, where the 'contamination'

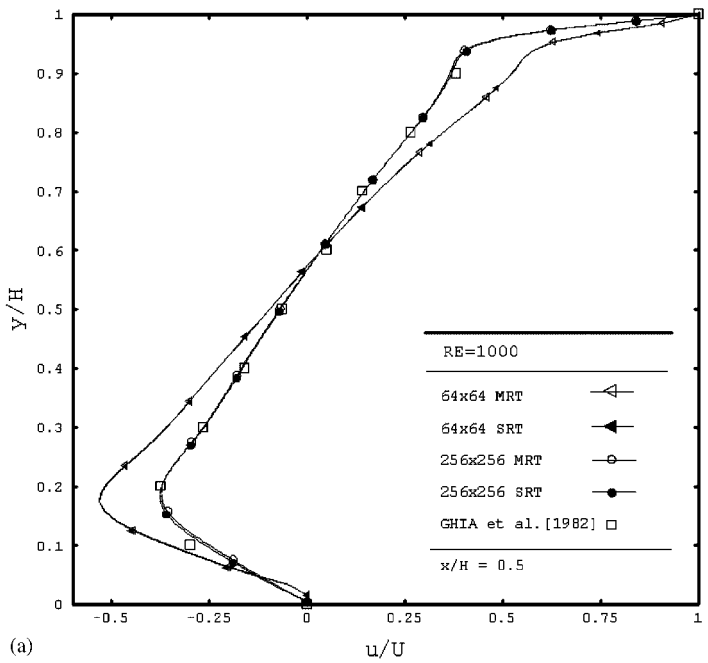

(a)

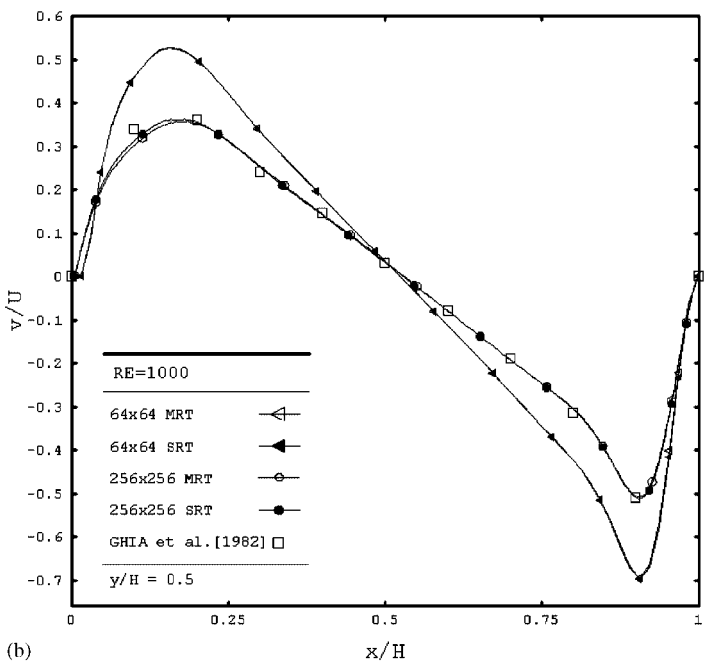

(b)

Figure 2. (a) Velocity profiles for u along the vertical geometric centreline of the cavity; (b) Velocity profiles for v along the horizontal geometric centreline of the cavity.

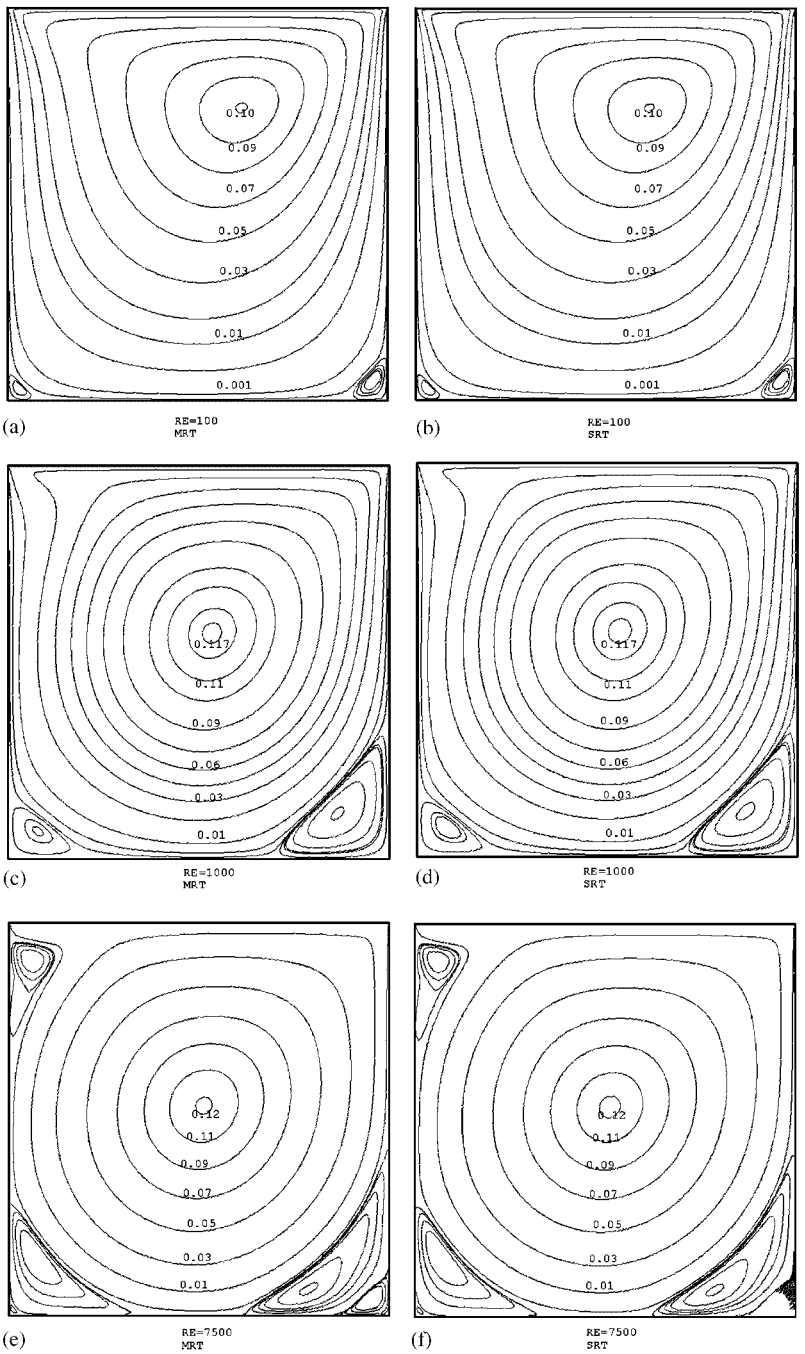

Figure 3. Streamline plot at various Reynolds numbers (a) $Re = 100$(MRT); (b) $Re = 100$(SRT); (c) $Re = 1000$(MRT); (d) $Re = 1000$(SRT); (e) $Re = 7500$(MRT); (f) $Re = 7500$(SRT).

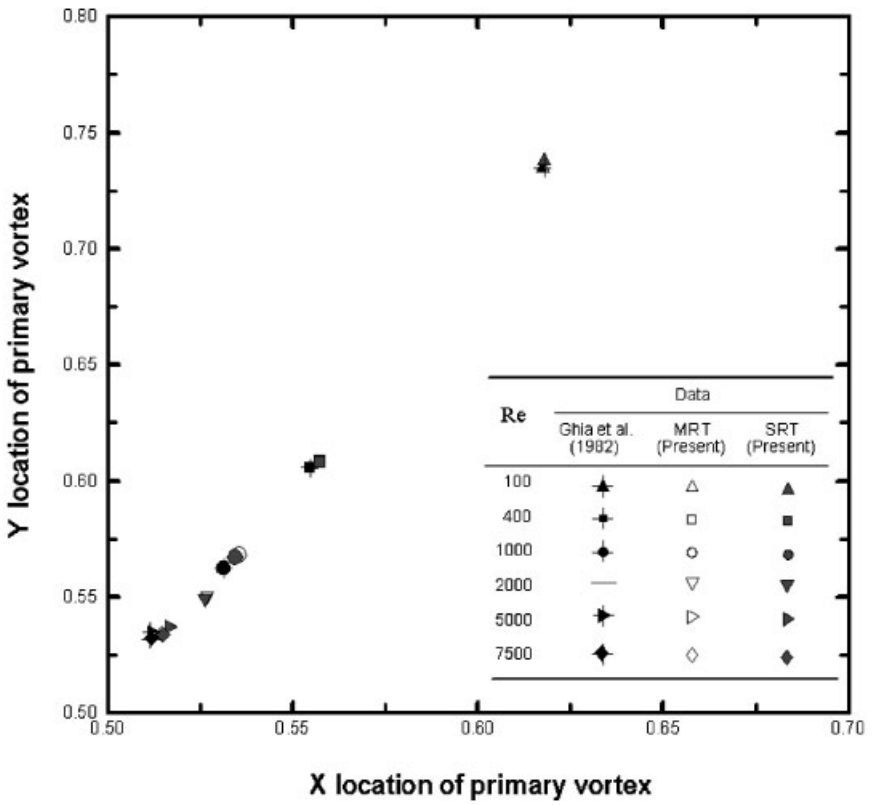

Figure 4. The location of the centre of the primary vortex for different values of Reynolds, SRT and MRT models.

Table I. Vortex centres: stream function for primary vortex.

	Reynolds number					
Primary vortex	100	400	1000	2000	5000	7500
a	0.1034	0.1139	0.1179		0.1190	0.1200
b	0.1031	0.1124	0.1171	0.1195	0.1201	0.1210
c	0.1030	0.1122	0.1170	0.1197	0.1203	0.1215

Note: a. U. Ghia, K.N. Ghia, and C. T. Shin [25]. b. MRT model (present). c. SRT model (present).

penetrates into the central part of the cavity using SRT model, although it is not shown in the current paper.

The above-mentioned differences for SRT and MRT models are highlighted again more clearly by the pressure contours at various Reynolds numbers as shown in Figure 6. The pressure deviation is defined as $c_s^2 \times (\rho - \bar{\rho})$, where $\bar{\rho}$ is the average fluid density of within the

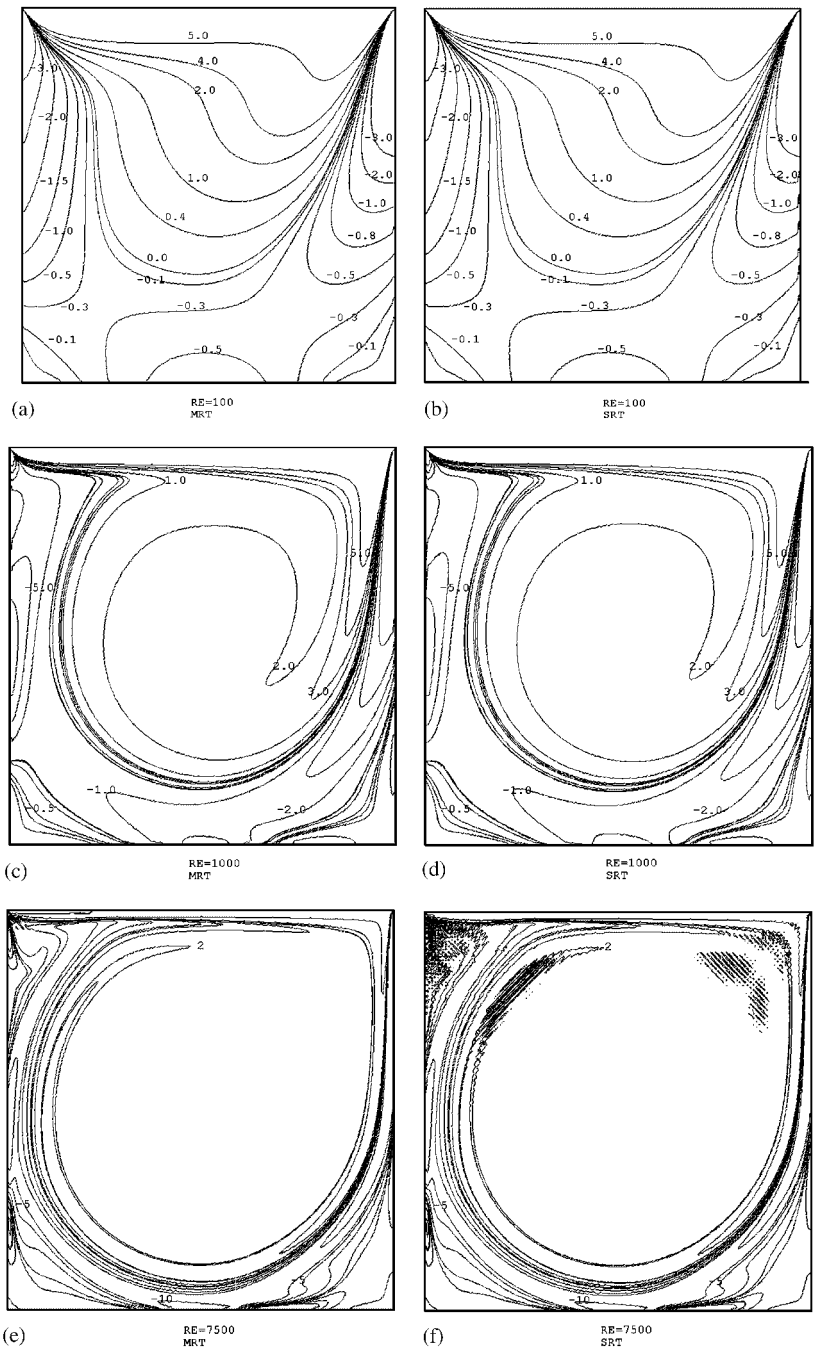

Figure 5. Contour plots of vorticity at various Reynolds numbers (a) $Re = 100$(MRT); (b) $Re = 100$ (SRT); (c) $Re = 1000$(MRT); (d) $Re = 1000$(SRT); (e) $Re = 7500$(MRT); (f) $Re = 7500$(SRT).

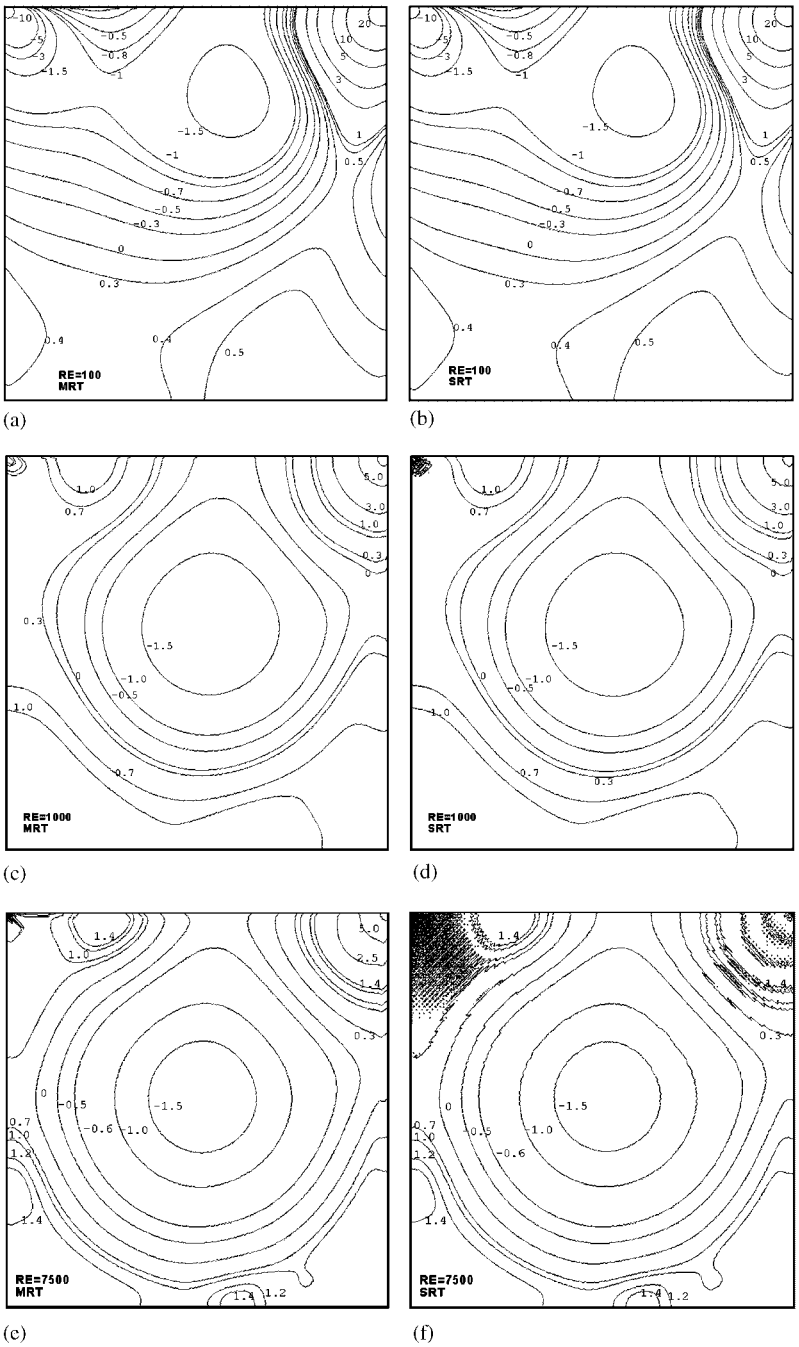

Figure 6. Normalized pressure contours at various Reynolds numbers (x 1000) (a) $Re = 100$(MRT); (b) $Re = 100$(SRT); (c) $Re = 1000$(MRT); (d) $Re = 1000$(SRT); (e) $Re = 7500$(MRT); (f) $Re = 7500$(SRT).

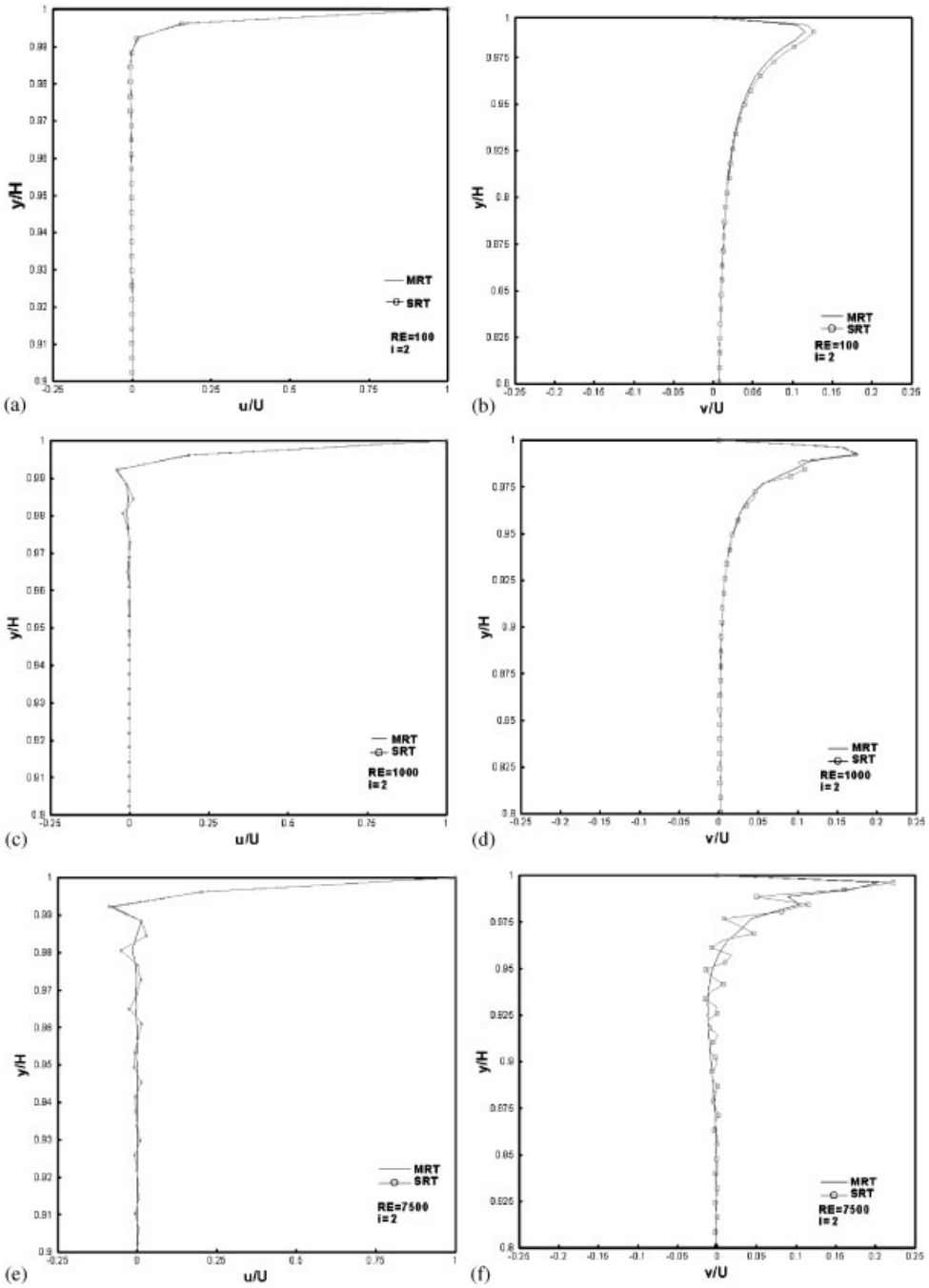

Figure 7. Comparison of the velocity profiles at various Reynolds numbers ($i = 2$) (a) $Re = 100$(x-component); (b) $Re = 100$(y-component); (c) $Re = 1000$ (x-component); (d) $Re = 1000$(y-component); (e) $Re = 7500$(x-component); (f) $Re = 7500$(y-component).

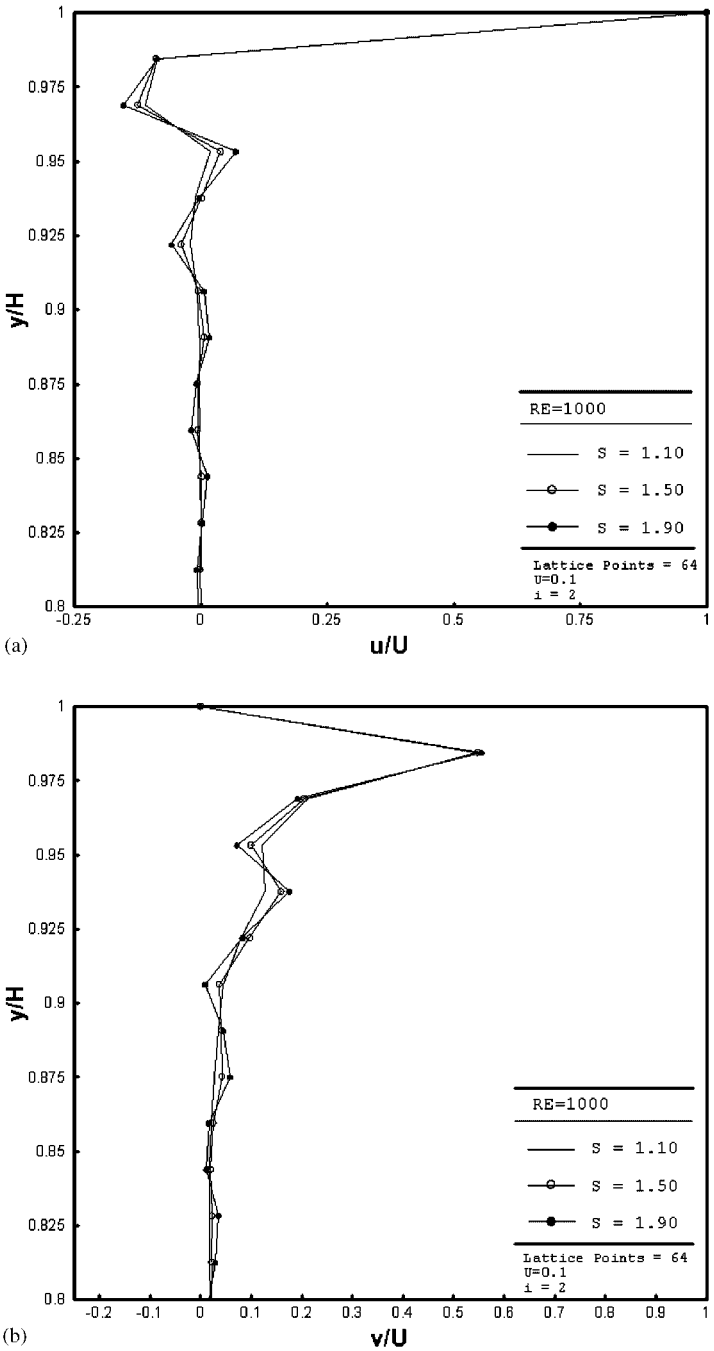

Figure 8. Sensitivity of the selecting relaxation parameters of the velocity profiles at $i = 2$ (a) x-component (b) y-component.

cavity. In these figures, values of pressure deviation are multiplied by 1000 for the purpose of illustration clarity. It can be seen that the pressure contour at the upper-left corner for SRT model becomes blurred at $Re = 1000$ (Figure 6(d)), which geometric singularity begins to influence the flow solution near this corner. The situation becomes worse even in regions far away from the corner at $Re = 7500$ for SRT model (Figure 6(f)), while the pressure contour remains normal at this Reynolds number for MRT model. The differences between SRT and MRT models can also be highlighted in detail later by considering the detailed distribution of velocity profiles near these corners as follows.

Figure 7 illustrates the comparison of u and v velocity distributions very close to the left vertical wall ($i = 2$ lattice point) for SRT and MRT models at various Reynolds numbers. Results clearly show that the velocity distributions (both u- and v-velocity) by SRT model present obvious spatial oscillations close to the upper-left corner, while the velocity distributions by MRT model present much less spatial oscillation in the same region of interest. In general, the spatial oscillation of solution around the upper-left corner becomes worse as Reynolds number increases. The difference represents that MRT model is more suitable, as compared with SRT model, for treating flow around geometrical singularity and potentially higher Reynolds-number flows, at least, for steady flows.

Finally, sensitivity of selecting the relaxation parameters (s_2, s_3, s_5 and s_7) has shown (Figure 8 for $Re = 1000$, 64×64 lattice points) to be relatively small once their values are close to 1.1. For values of the relaxation parameters close to 1.9, the spatial oscillations of the u- and v-velocity appear to be serious. Also the deviation increases with increasing Reynolds number as expected. Note that for the results presented in the above, they are all set to 1.1 for the simplicity, unless otherwise specified.

4. CONCLUSIONS

In the current study, an upper, lid-driven cavity flow is simulated by parallel lattice Boltzmann method using multi-relaxation time scheme. Results are then compared with those by LBM using single-relaxation time scheme and previous published data using N–S solver. In general, results using MRT and SRT techniques are both in good agreement with those using N–S solver for $Re = 100$–7500 for the most part of the flow within the cavity. In summary, we can conclude that MRT technique is superior to SRT technique in simulating higher Reynolds number flows having geometrical singularity with much less spatial oscillations due to the different relaxation rates for different physical modes embedded in the MRT scheme. In addition, the code using the MRT model takes only about 15% more CPU time than that using SRT model. Test for unsteady (periodic) flow, e.g. a flow past an obstacle with vortex shedding using MRT technique is currently in progress and will be reported in the near future.

ACKNOWLEDGEMENTS

Authors would like to thank Dr. Bersdoff and Dr. Li-Shi Luo for helpful discussions during the initial development of this research. Parallel computing resources partly provided by National Center for High-performance Computing in Taiwan is also highly appreciated.

REFERENCES

1. Higuera FJ, Jeminez J. Boltzmann approach to lattice gas simulations. *Europhysics Letters* 1989; **9**:663–668.
2. Higuera FJ, Succi S, Benzi R. Lattice gas-dynamics with enhanced collisions. *Europhysics Letters* 1989; **9**:345–349.
3. Succi S, Amati G, Benzi R. Challenges in lattice Boltzmann computing. *Journal of Statistical Physics* 1995; **81**:5–16.
4. Qian YH, Succi S, Orszag SA. Recent advances in lattice Boltzmann computing. *Annual Review of Computational Physics*, vol. III. World Scientific: Singapore, 1995; 195–242.
5. Chen S, Doolen GD. Lattice Boltzmann method for fluid flow. *Annual Review of Fluid Mechanics* 1998; **30**:329–364.
6. Bhatnagar PL, Gross EP, Krook M. A model for collision proceses in gases. I. Small amplitude processes in charged and neutral pn-component system. *Physical Review* 1954; **94**:511–525.
7. Chen H, Chen S, Matthaeus WH. Recovery of the Navier–Stokes equations using a lattice Boltzmann method. *Physical Review A* 1992; **45**:R5339–R5342.
8. Kandhai D, Koponen A, Hoekstra A, Kataja M, Timonen J, Sloot PMA. Lattice Boltzmann hydrodynamics on parallel systems. *Computer Physics Communications* 1998; **111**:14–26.
9. Dieter A, Wolf-Gladrow. *Lattice Gas Cellular Automata and Lattice Boltzmann Models*. Springer: Berlin, 2000.
10. Krafczyk M, Schulz M, Rank E. Lattice-gas simulations of two-phase flow in porous media. *Communications in Numerical Methods in Engineering* 1998; **14**:7–12.
11. Bernsdorf J, Brenner G, Durst F. Numerical analysis of the pressure drop in porous media flow with lattice Boltzmann (BGK) automata. *Computer Physics Communications* 2001; **129**:247–255.
12. Freed DM. Lattice-Boltzmann method for macroscopic porous media modeling. *International Journal of Modern Physics C* 1998; **9**:1491–1503.
13. Kono K, Ishizuka T, Tsuba H. Application of lattice Boltzmann model to multiphase flows with phase transition. *Computer Physics Communications* 2001; **129**:110–120.
14. Hou S, Shan X, Zou Q, Doolen GD, Soll WE. Evaluation of two lattice Boltzmann models of multiphase flows. *Journal of Computation Physics* 1997; **138**:695–713.
15. He X, Chen S, Zhang R. A lattice Boltzmann scheme for incompressible multiphase flow and its application in simulation of Rayleigh Taylor instability. *Journal of Computation Physics* 1999; **152**:642–663.
16. Hashimoto Y, Ohashi Y. Droplet dynamics using the lattice-gas method. *International Journal of Modern Physics C* 1997; **8**:977–983.
17. Xi H, Duncan C. Lattice Boltzmann simulations of three-dimensional single droplet deformation and breakup under simple shear flow. *Physical Review E* 1999; **59**:3022–3026.
18. Hou S. Lattice Boltzmann Method for Incompressible, Viscous Flow. *Ph.D. Thesis*, Department of Mechanical Engineering, Kansas State University, 1995.
19. D'Humieres D. Generalized lattice Boltzmann equation. In *Rarefied Gas Dynamics*: *Theory and Simulations*, *Progress in Astronautics and Aeronautics*, vol. 159, Shizgal BD, Weaver DP (eds). AIAA: Washington, DC, 1992; 45–458.
20. Lallemand P, Luo L-S. Theory of the lattice Boltzmann method: dispersion, dissipation, isotropy, Galilean invariance, and stability. *Physics Review E* 2000; **61**:6546–6562.
21. Inamuro T, Yoshine M, Ogino F. A non-slip boundary condition for lattice-Boltzmann simulations. *Physics of Fluids* 1995; **7**:2928–2930.
22. Ghia U, Ghia KN, Shin CT. High-Re solutions for incompressible flow using the Navier–Stokes equations and a multigrid method. *Journal of Computational Physics* 1982; **48**:387–411.
23. Davis RW, Moore EF, Putell LP. A numerical–experimental study of confined flow around rectangular cylinders. *Physics of Fluids* 1984; **27**:46–59.
24. Wolf-Gladrow DA. *Lattice-Gas Cellular Automata and Lattice Boltzmann Models*. Springer: Berlin, 2000.
25. Bruer M, Bernsdorf J, Zeiser, Durst F. Accurate computations of the laminar flow past a square cylinder based on two different methods: lattice-Boltzmann and finite-volume. *International Journal of Heat and Fluid Flow* 2000; **21**:186–196.

